SPE-205936-MS

An Efficient Hydraulic Fracture Geometry Calibration Workflow Using Microseismic Data, Geomechanics, DFN Models, and History Matching

Joseph Alexander Leines-Artieda, SimTech LLC; Chuxi Liu, The University of Texas at Austin; Hongzhi Yang, Jianfa Wu, and Cheng Chang, Petrochina Southwest Oil&Gas Field Company; Wei Yu, SimTech LLC; Kamy Sepehrnoori, The University of Texas at Austin

This paper was prepared for presentation at the 2021 SPE Annual Technical Conference and Exhibition held in Dubai, UAE, 21 - 23 September 2021.

Abstract

Reliable estimates of hydraulic fracture geometry help reduce the uncertainty associated with estimated ultimate recovery (EUR) forecasts and optimize field developing planning in unconventional reservoirs. For these reasons, operators gather information from different sources with the objective to calibrate their hydraulic fracture models. Microseismic data is commonly acquired by operators to estimate hydraulic fracture geometry and to optimize well completion designs. However, relying solely on estimates derived from microseismic information may lead to inaccurate estimates of hydraulic fracture geometry.

The objective of this study is to efficiently calibrate hydraulic fracture geometry by using microseismic data, physics-based fracture propagation models, and the embedded discrete fracture model (EDFM). We first obtain preliminary estimates of fracture geometry based on microseismic events' spatial location and density with respect to the perforation cluster location. We then tune key completion parameters using an in-house fracture propagation model to provide hydraulic fracture geometries that are constrained by the microseismic cloud. In the history matching process, we included the effect of natural fractures, using the microseismic events location as natural fracture initiation points. Finally, we used cutoff coefficients to further reduce hydraulic fracture geometries to match production data.

The results of this work showed a fast and flexible method to estimate fracture half-lengths and fracture heights, resulting in a direct indicator of the completion design. Additionally, hydraulic-natural fracture interactions were assessed. We concluded that the inclusion of cutoff coefficients as history matching parameters allows to derive realistic hydraulic and natural fracture models calibrated with microseismic and production data in unconventional reservoirs.

Introduction

Hydraulic fracture propagation models are commonly used to obtain hydraulic fracture geometries by linking completion information from the hydraulic fracture treatment with the geomechanical features of the reservoir (Virues and Iheanyichukwu, 2016; Xie et al., 2020). Such fracture propagation models depend on certain input parameters that may generate underestimated or overestimated representations of fracture

geometries if further information is not used to reduce their uncertainty. Leak-off coefficient is a critical parameter that determines the fracture extension in the stimulation job (Ghaderi et al., 2019). However, this parameter cannot be directly measured in the field, which adds to the fracture propagation model results' uncertainty. Other parameters that can alter fracture geometry are Young's modulus, fracture toughness, and the stress state in the reservoir, which are also highly variable due to reservoir anysotropy and layering effects (Yuan et al., 2017; Suo et al., 2020).

Recently, advancements in unconventional reservoirs have allowed the integration of several sources of information to help optimize fracturing jobs and reduce the uncertainty associated with fracture geometries. Microseismic data, distributed temperature sensing (DTS), distributed acoustic sensing (DAS), and distributed strain sensing (DSS) are excellent sources of information that can be used to understand and improve completion jobs (Sun et al., 2020; Hull et al., 2020; Jin et al., 2021). Among those sources of information, microseismic data is more present than its other counterparts. While it is true that microseismic data possesses certain amount of uncertainty, due to microseismic resolution, it still can provide reliable guidelines of hydraulic fracture extension in unconventional reservoirs.

Microseismic data responds to the activation, due to shear slip caused by elevated pore pressure during the fracturing job, of pre-existing natural fractures or faults in the reservoir (Rutledge et al., 2016; Hakso and Zoback, 2019). Depending on the reservoir architecture, the stimulation process can activate geological features located far away from the main stimulated region. Consequently, using the entire microseismic cloud to directly obtain gross estimates of the stimulated reservoir volume (SRV) or fracture half-lengths and heights can lead to misleading estimates due to certain events could be associated with activation of failure planes unrelated with the stimulation job.

Production data can also be used to further calibrate hydraulic fracture geometries. In order to support a reliable estimation of the production behavior, history matching is an excellent tool to help engineers characterize hydraulic fractures and reservoir properties. Dual porosity dual permeability (DPDK) models have been traditionally used to model hydraulic fractures in unconventional reservoirs; however, one key drawback is the overestimation of fracture connectivity when fractures are not fully connected in 3D (Kumar et al., 2019). When including natural fractures in the reservoir model, the DPDK method may overestimate their contribution if the fractures are isolated. Unstructured grids also are commonly used to model hydraulic fractures, but they suffer from high computational costs due to excessive gridblocks to conform to hydraulic fractures. Local grid refinement is another mechanism to model hydraulic fractures (Cipolla et al., 2010); however, fracture orientations are challenging to be represented, resulting in increased computational costs. In the last two methods, including complex natural fractures could further increase the computational cost, resulting in unfeasible models at the field scale. The embedded discrete fracture model (EDFM), on the other hand, has proved to be an efficient mechanism to accurately model hydraulic and natural fractures while preserving their geometries and orientations.

The method discretizes the fractures in a different domain and calculate transport indices using three different types of connections between matrix-matrix, fracture segments, and fractures-fractures (Xu et al., 2017). Fig. 1 describes the EDFM method in more detail. The method is flexible and allows to link fracture models with reservoir simulators to be used for history matching purposes. In this work, we use microseismic data to constrain fracture geometry generated from fracture propagation models. The results are then further calibrated using cutoff coefficients in order to match production data in an unconventional shale gas well.

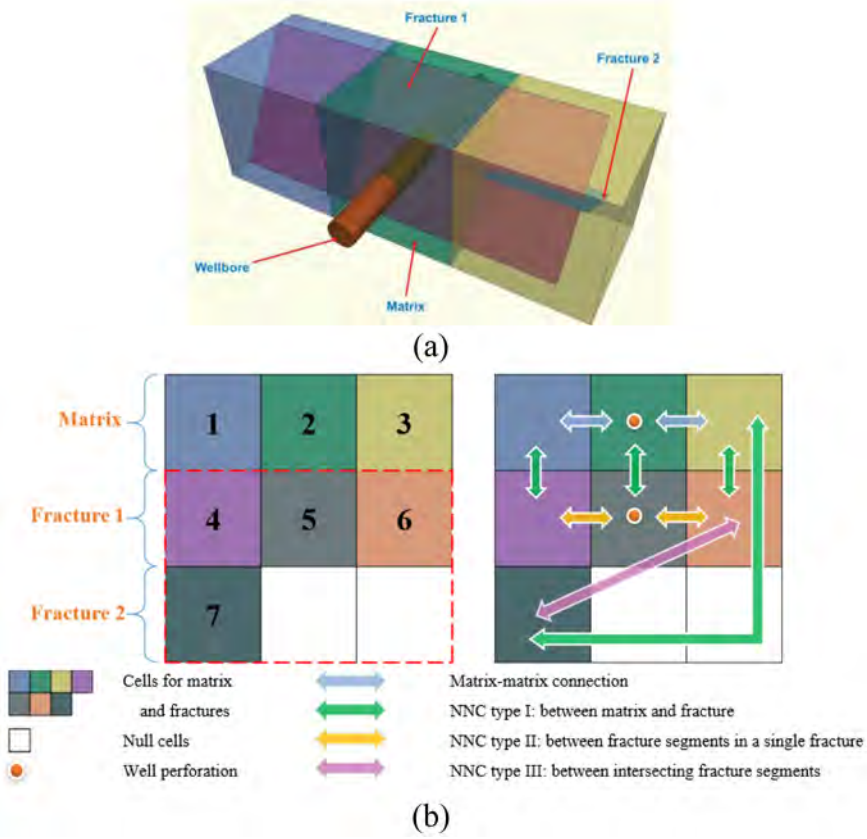

Figure 1—General description of embedded discrete fracture model (EDFM): (a) a physical domain with three matrix blocks, two fractures, and a wellbore; and (b) a computational domain showing the different types of non-neighboring connections (NNCs) (Xu et al., 2017).

Methods

The first step of our workflow revolves around determining estimates of fracture extension using microseismic data. For this reason, we developed a guiding fracture plane generator to help automatically constrain fracture dimensions at the cluster level. The method creates dummy planes generated orthogonally to the well trajectory using cluster coordinates as initiation points. Then, microseismic events are grouped by their closeness to each perforation cluster. Clusters with fewer number of events than a constant parameter were merged with nearby cluster with less density, forming one single cluster whose initiation point becomes the middle point between both clusters. After this phase, the algorithm discards events located outside the targeted reservoir thickness. As a result, fracture half-length per stage is calculated by averaging the projected distances from each perforation coordinate to the distance of the farthest microseismic event in each cluster. Fracture height is calculated as the difference between the z-coordinate of the upper-most and lowest-most microseismic event in each cluster. Fig. 2 illustrates the guiding fracture planes obtained along with the microseismic data.

Th next step is to provide the initial estimates of hydraulic fracture half-length and height to the fracture propagation model to calibrate fracture growth. Reservoir properties, geomechanical information, and completion information are needed to generate a representative fracture model of the multistage hydraulic fracturing job using an in-house hydraulic fracture propagation model (Wu and Olson, 2015). The model couples rock deformation and fluid flow in the fractures and the wellbore. In order to honor computational efficiency, a pseudo-3D model and a simplified three-dimensional displacement discontinuity method (simplified 3D-DDM) were used in this case study. Subsequently, geomechanical parameters (leak-off coefficient, fracture toughness, and main layer height) are tuned to obtain the hydraulic fracture model that is constrained by the initial estimates of fracture geometry given by the microseismic information.

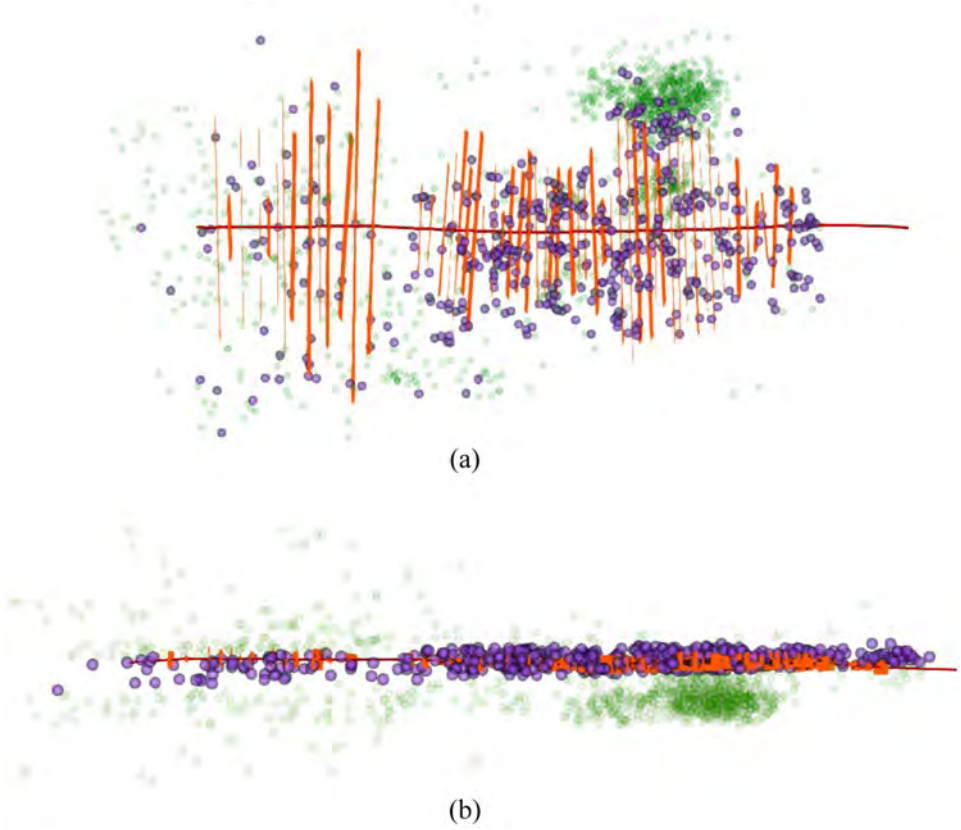

Figure 2—Guiding fracture planes generated from microseismic data (orange) and microseismic events (purple, screened out events inside the reservoir region; green, whole microseismic cloud): (a) Plan view of the model; (b) side view of the model.

Natural fracture activation can be modeled by using an in-house discrete fracture network (DFN) generator. We assume the microseismic events location as natural fracture initiation points. Natural fracture orientation and geometry can be estimated from image logs and history matching results from nearby wells.

Connecting fracture models with production data is possible thanks to an in-house fracture cut-off algorithm that efficiently reduces fracture geometry using cutoff coefficients. Two cutoff coefficients are involved, which reduce fracture half-lengths and heights, respectively. If the cutoff coefficients are used as history matching parameters, the fracture geometries can be further modified on-the-fly in order to match production data. Additionally, hydraulic and natural fracture interactions are evaluated at each variation of the hydraulic fracture geometry, resulting in a robust mechanism to evaluate the impact of natural fractures activation and its response on production behavior. A summary of the general workflow is illustrated in Fig. 3.

Case study

In this case study, microseismic data was acquired by the operator during the fracture stimulation job. The well lateral length is 1500 m. and was completed with 23 stages and 3 clusters per stage, resulting in 69 clusters. Information regarding the stress state in the reservoir was gathered along with some reservoir geomechanical properties, which are shown in Table 1. We further proceeded to obtain the guiding fracture planes, which provided initial estimates of fracture half-lengths and height. Subsequently, we run the fracture propagation model to simulate the multi-stage fracture propagation growth using the initial fracture geometry as constraint parameters. We tuned the geomechanical parameters of each stage until the hydraulic fracture extension is similar to the guiding fracture planes. Fig. 4 shows how the fracture propagation model (blue) is constrained inside the guiding fracture planes (orange) obtained from microseismic information. Regions with no guiding planes result from minor microseismic activity.

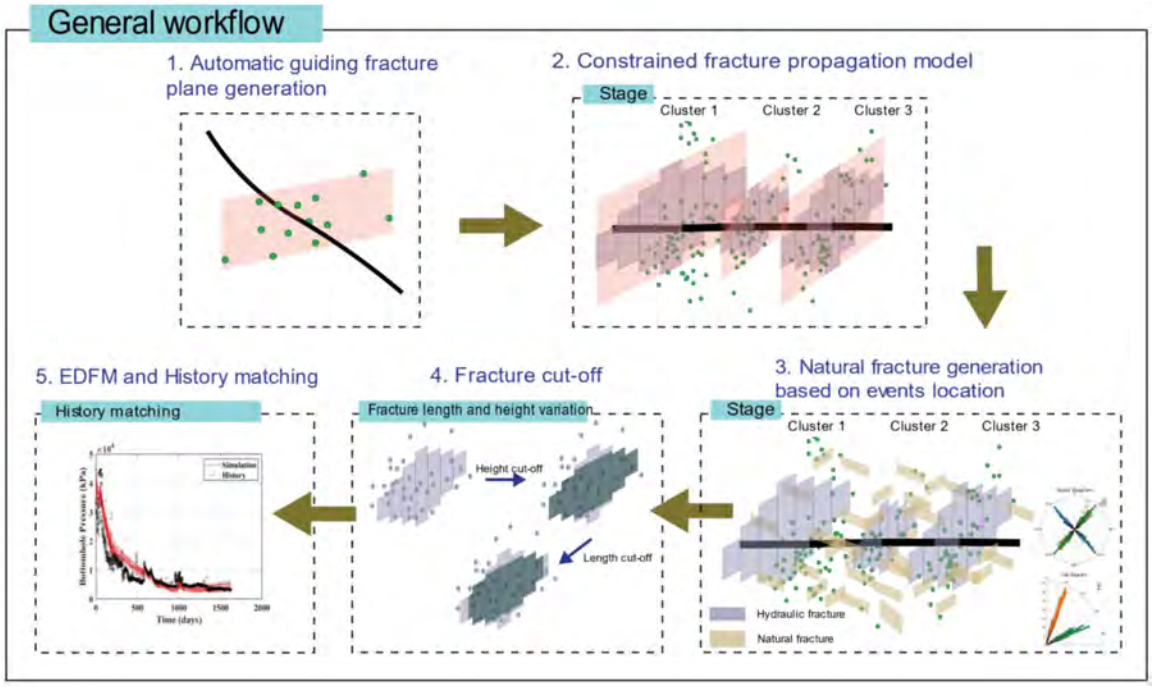

Figure 3—General description of the microseismic-geomechanics-simulation workflow, consisting in 5 steps. Guiding fracture plane generation is the first step, which is continued by generating hydraulic fractures using a fracture propagation model. Natural fractures are added to the model and history matching is performed using cutoff coefficients.

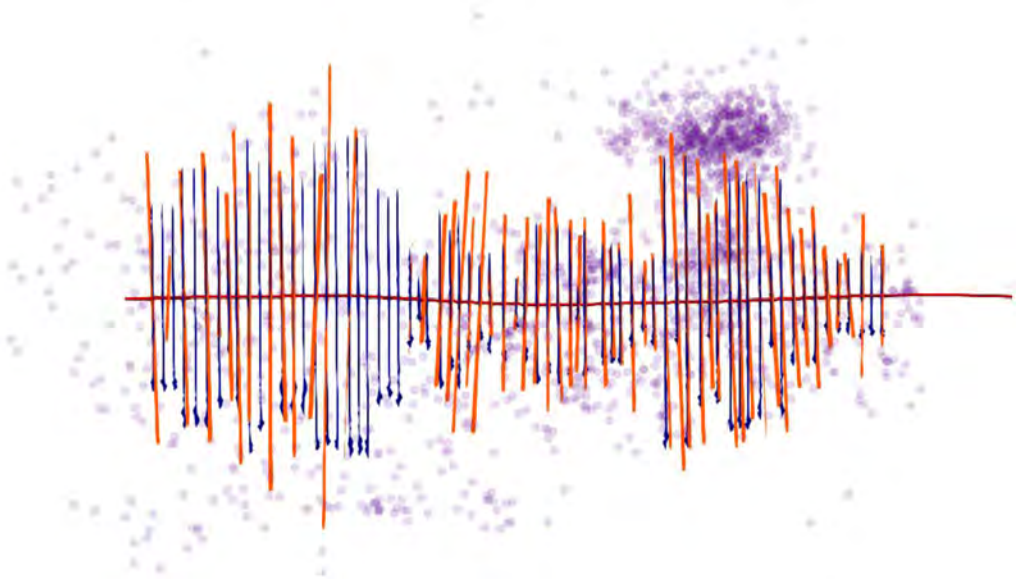

Figure 4—Hydraulic fractures constrained by microseismic data. Guiding fracture planes are shown in orange, and hydraulic fractures from the fracture propagation model are shown in blue; the original microseismic cloud is shown in purple.

Table 1—Geomechanical properties used in the shale-gas fracture propagation model.

Reservoir Description	Value	Unit
S_{hmin}	86	MPa
S_{hmax}	98	MPa
Layer toughness	1	MPa×m$^{0.5}$
Young's modulus	46	GPa
Poisson ratio	0.24	-

Dynamic information of initial 334 days of production of the shale gas well under study was available. The reservoir model dimensions are 1000 × 2200 × 76 m. The number of gridblocks used, in a corner point grid, is 64 × 144 × 10, resulting in grid block dimensions of 15 × 15 m. in x- and y- directions, respectively. A detailed description of all the reservoir parameters is shown in Table 2. Fig. 5a and Fig. 5c show the corner point grid used for this study case, which was populated with different layer properties. Fig. 5b shows the DFN model generated using microseismic events located inside the reservoir model. Natural fracture orientation was obtained from nearby well image logs, and their geometry was estimated using nearby history matched wells. Two natural fracture sets were found to coexist in the reservoir: set one, presenting average fracture strike of 275° and fracture dip of 22°; and set two, presenting average fracture strike of 80° and fracture dip angle of 5°. Natural fracture geometry follows a power law distribution, whose minimum and maximum values are 48 and 110 m., respectively.

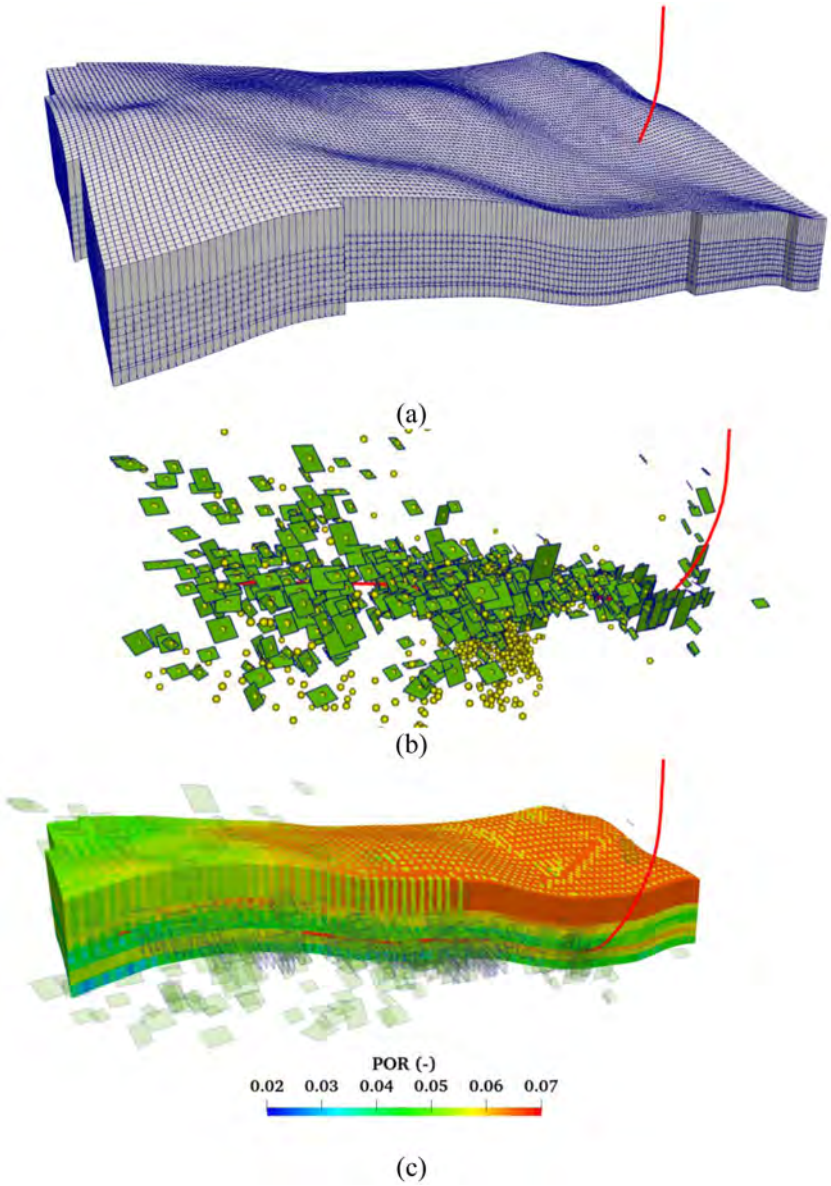

Figure 5—A shale-gas corner point reservoir model with complex natural fractures: (a) 3D corner point reservoir model with different layer properties; (b) complex natural fracture DFN generated from microseismic events; and (c) cross section of porosity heterogeneity parallel to well direction.

Table 2—Reservoir and fracture properties used in the field-scale shale-gas model.

Reservoir Description	Value	Unit
Model dimension (x × y × z)	1000 × 2200 × 76	m
Number of grid blocks (x × y × z)	64 × 144 × 10	-
Grid blocks dimensions (x × y)	15 × 15	m
Well depth	3660~3722	m
Well length	1500	m
Initial reservoir pressure	70	MPa
Reservoir temperature	150	◦C
Matrix water saturation	0.3	-
Water compressibility	6.18×10^{-4}	MPa^{-1}
Reference pressure for compressibility	0.101	MPa
Number of clusters	69	-
Number of stages	23	-
k°_{rw}	0.758	-
k°_{rg}	1.0	-
S_{wirr}	0.3	-
S_{gr}	0.1	-
n_w	3.09	-
n_g	2.86	-

We attempted to history match two cases: (1) without cutoff coefficients and (2) with cutoff coefficients to observe discrepancies in the well production behavior. We used gas rate as a constraint parameter for both cases and matched bottom-hole pressure (BHP) and water flow rate. Fig. 6a and Fig. 6b show the scenario without using cutoff coefficients, preserving the original results from the hydraulic fracture propagation simulator, which are constrained by the microseismic cloud. In contrast, Fig. 6c and Fig. 6d show the fracture geometry attained by using cutoff coefficients, which reduce the fracture geometry in both length and height directions. Additionally, Fig. 7 shows the full reservoir model including the DFN generated for both cases. We can clearly observe significant differences between both fracture models. The original model presents a larger fracture geometry with more physical interactions with natural fractures because it occupies more 3D space. However, the cutoff model presents a smaller fracture geometry with less hydraulic-natural fracture interactions. Natural fracture contribution was assessed for both cases, and its conductivity was used as a history matching parameter. It is worthwhile to mention that EDFM efficiently calculates the contribution of natural fractures to well performance because it considers natural fracture spatial and conductivity properties.

The history matching results for both cases are presented in Fig. 8. The fracture model without cutoff coefficients was not possible to match because it overestimates the hydraulic fracture geometry and, consequently, the production response. Both BHP and water flow rate present large discrepancies with respect to the case with cutoff coefficients, highlighting the necessity of including a reliable mechanism to tune fracture geometry even after using fracture propagation models. Fracture geometries attained using both methods are shown in Fig. 9. Key reservoir parameters such as matrix permeability and vertical permeability multiplier were characterized along with fracture geometry and natural fracture conductivity. Despite natural fracture contribution decreasing with time, caused mainly by natural fracture closure due to stresses, high number of hydraulic-natural fracture interactions may contribute to the overestimation of the fracture network influence in the first case. Original fracture height was reduced by 50% and fracture half-length

by 40% in order to match production data. Fracture closure at the fracture tip after the hydraulic fracture fully propagated may be one of the key reasons why fracture length in reality is smaller. Fracture height reductions may obey to gravitational settlement of proppant, which occupies lower regions of hydraulic fractures. All results of the history matching using cutoff coefficients are summarized in Table 3.

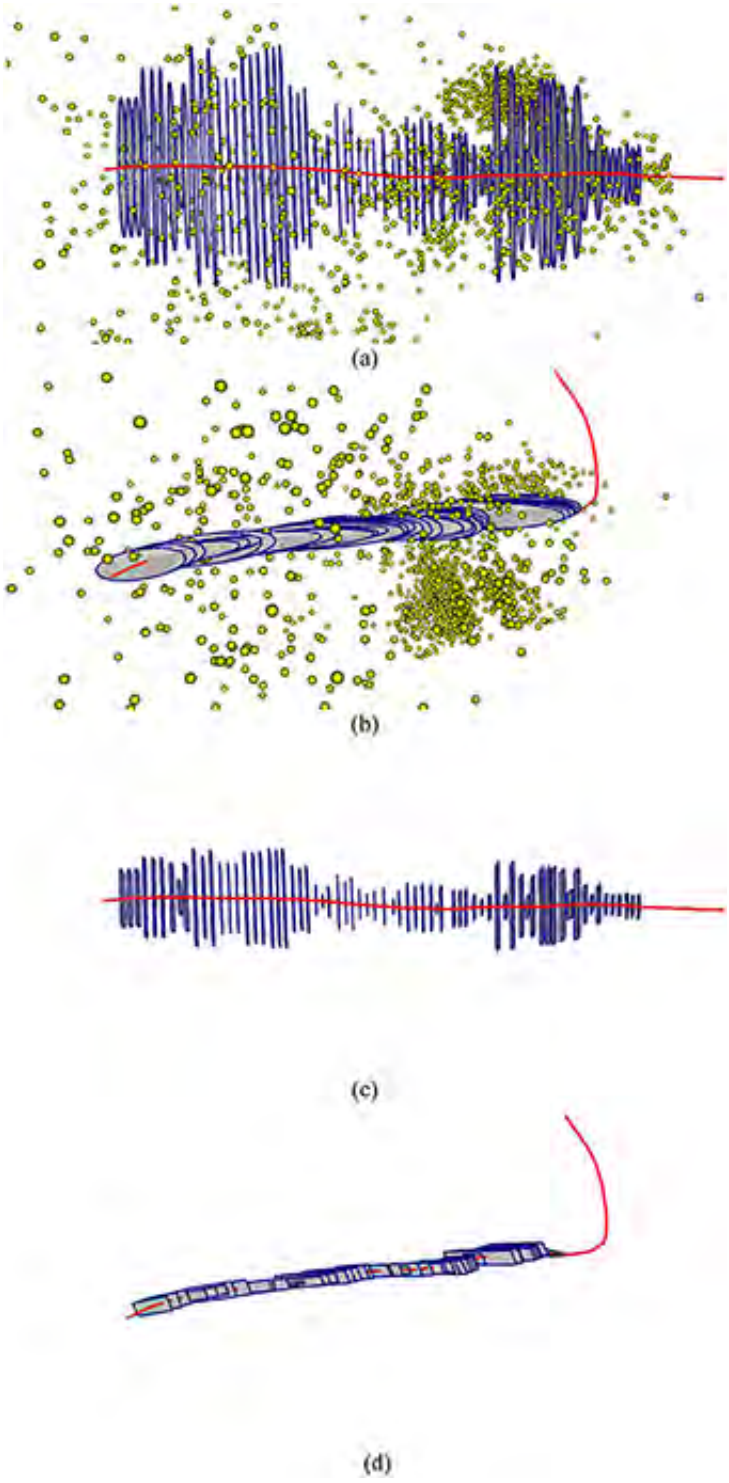

Figure 6—Visualization of complex hydraulic fractures geometries constrained first by microseismic events and by actual production history: (a) top view, fracture propagation model output before cutoff, constrained by microseismic events; (b) side view, fracture propagation model output before cutoff, constrained by microseismic events; (c) top view, after production calibration cutoff; and (d) side view, after production calibration cutoff

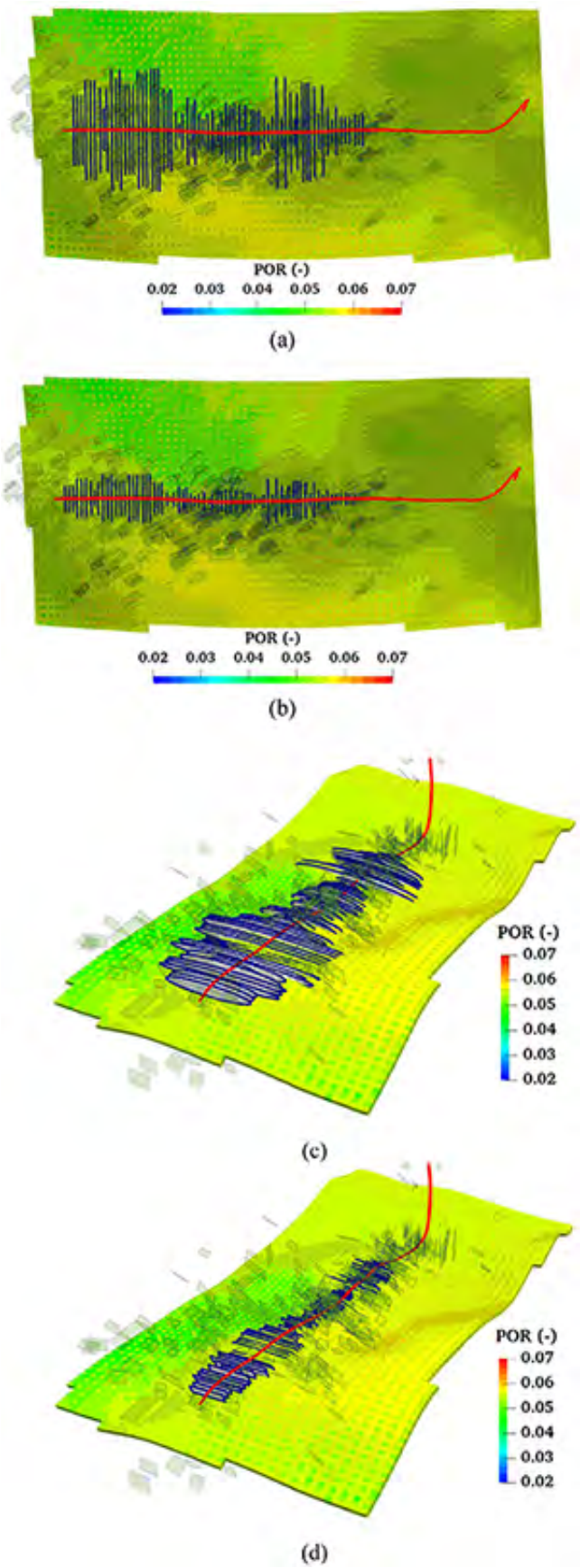

Figure 7—General visualizations of 2D and 3D reservoir/fracture model: (a) 2D before cutoff; (b) 2D after cutoff; (c) 3D before cutoff; and (d) 3D after cutoff

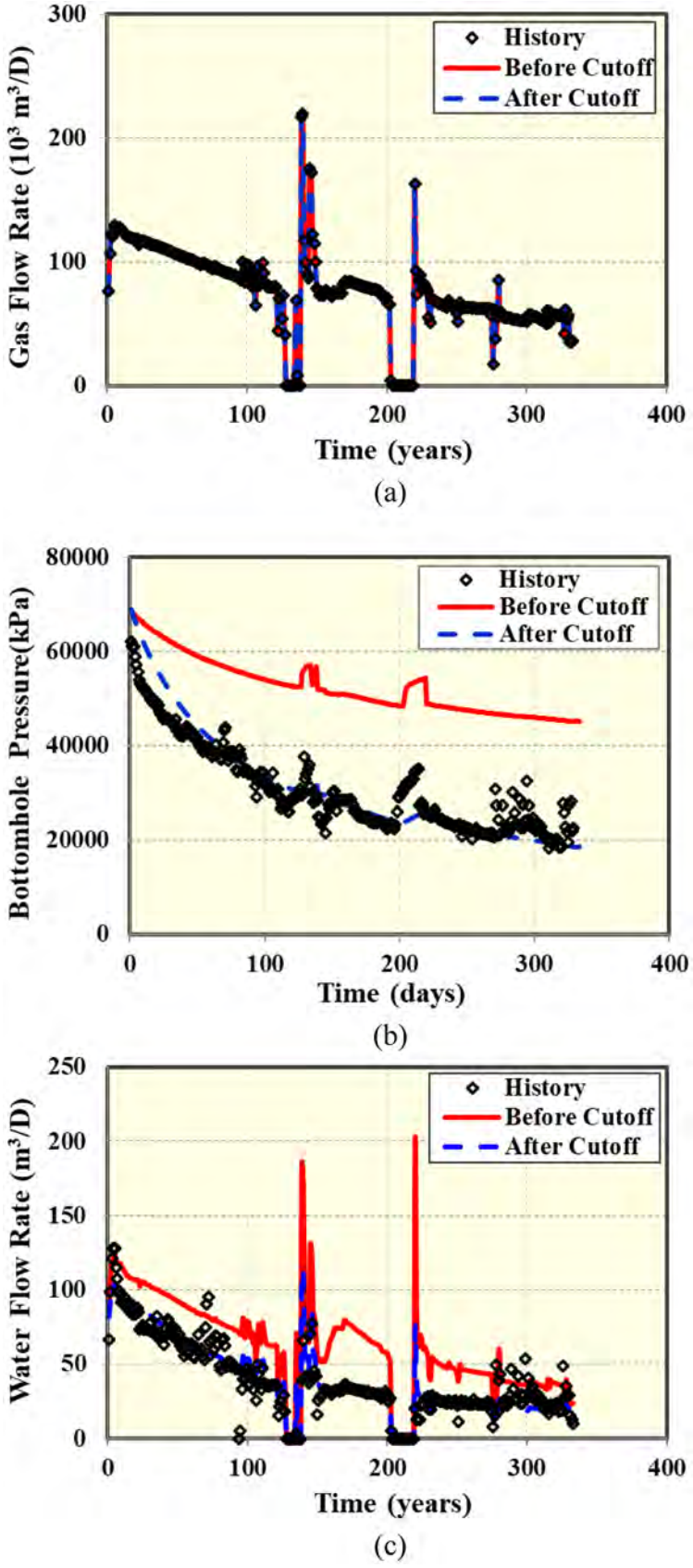

Figure 8—History matching constraint and results comparing before and after cutoff calibration against history data: (a) gas flow rate as constraint; (b) BHP matching results; (c) water flow rate matching results.

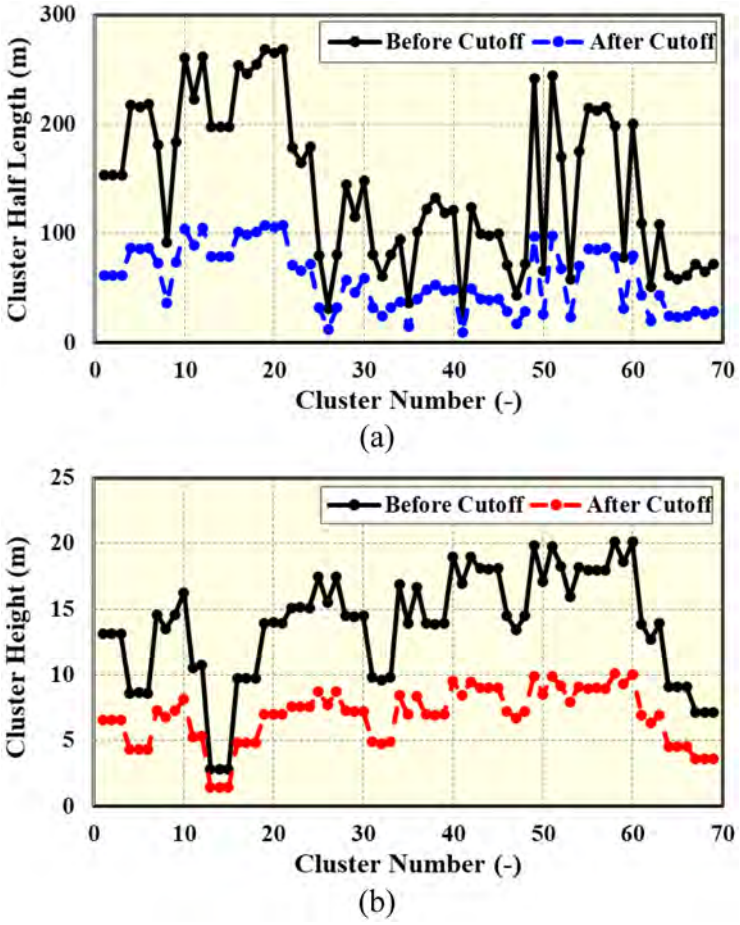

Figure 9—Complex fracture geometries before and after cutoff calibration: (a) hydraulic fracture half-lengths; and (b) hydraulic fracture heights.

Table 3—Summary of best match values for different uncertainty parameters

Uncertain Parameters	Cutoff Calibration	Unit
Matrix permeability	45.2	nd
Vertical permeability multiplier	0.001	-
Fracture height cutoff coefficient	50%	-
Fracture half-length cutoff coefficient	40%	-
Fracture closure coefficient	0.0202	-
Fracture water saturation	0.744	-
Hydraulic fracture conductivity	26.9	md-m
Natural fracture conductivity	0.384	md-m

We conducted long-term EUR forecasting for both cases. We used both the representative best match of the original fracture geometry and the cutoff fracture geometry. We simulated 20-year production time, and we used a minimum bottomhole pressure of 1500 kPa as the long-term constraint for the prediction in both scenarios. BHP constraint and cumulative gas/water production for both scenarios are included in Fig. 10. For the original fracture geometry scenario, the figure shows that the 20-year gas EUR and 20-year water EUR are larger, compared with cutoff fracture geometry scenario. Values of gas/water EUR for both scenarios are 209 million standard cubic feet (MMSCF) / 112 MSTB and 102 MMSCF / 30 MSTB, respectively. Fig. 11 shows the drainage volume for both cases, highlighting the overestimation of fracture

geometry after 334 days, 5 years, and 20 years of production. Additionally, we included pressure drawdown visualizations (Fig. 12) to observe the pronounced effect of pressure drawdown in the original fracture geometry case in comparison to the cutoff fracture geometry case at different times.

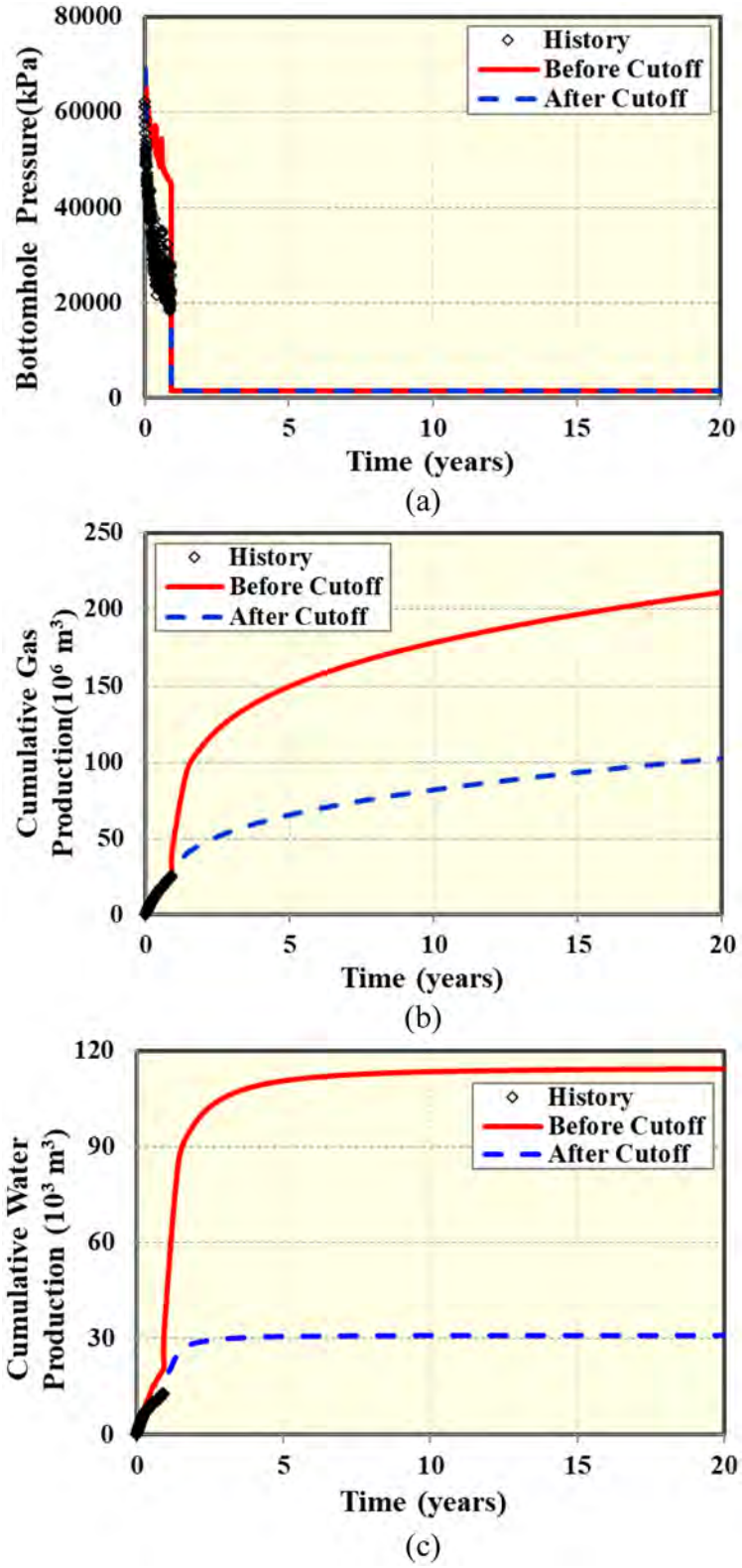

Figure 10—Twenty years production forecast constraint and results comparing before and after cutoff results: (a) direct dropdown of BHP as prediction constraint; (b) cumulative gas production; (c) cumulative water production.

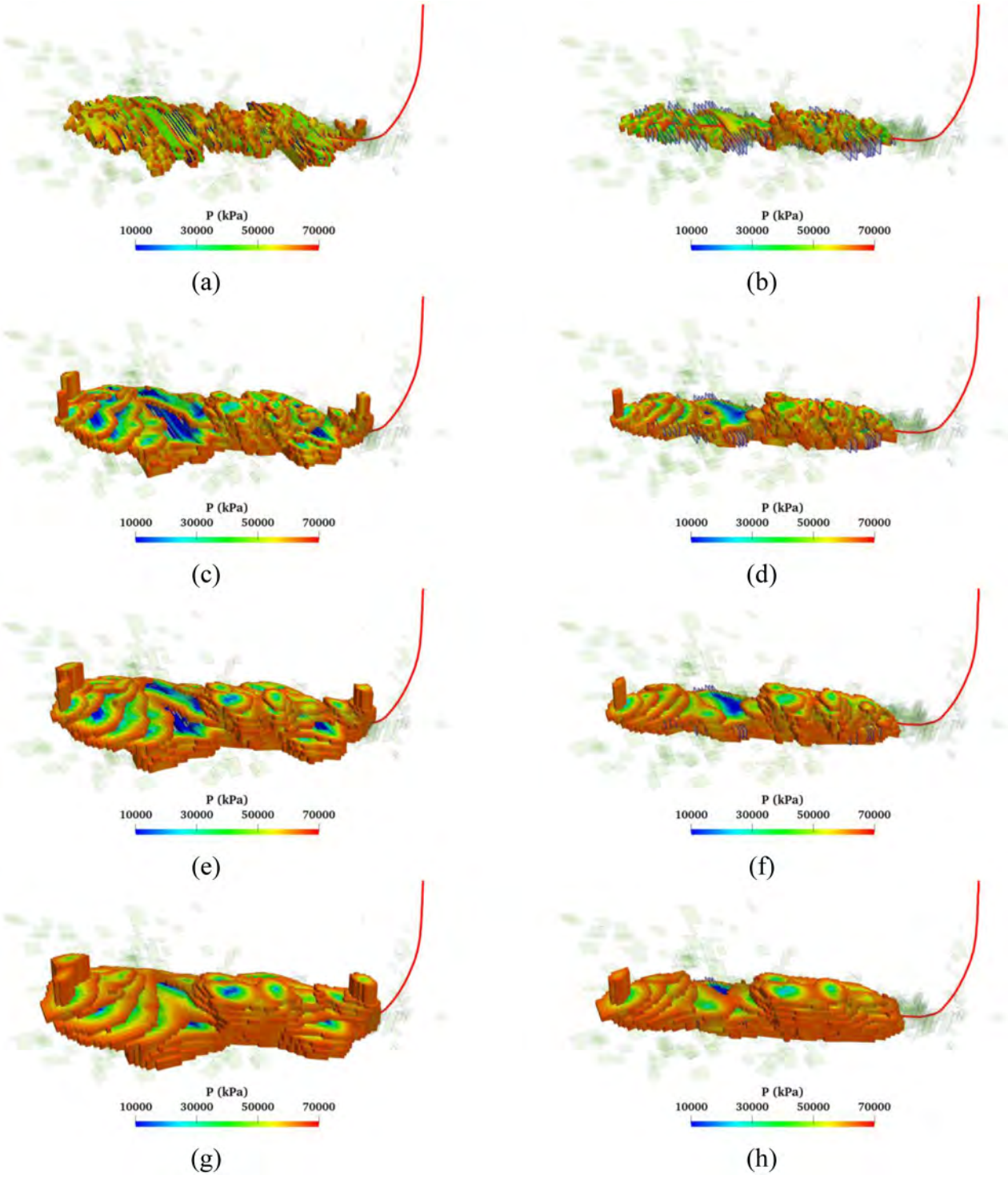

Figure 11—Comparison of drainage volume visualizations at different time before and after cutoff calibration: (a) before cutoff at end of history (334 days); (b) after cutoff at end of history (334 days); (c) before cutoff at 5 years; (d) after cutoff at 5 years; (e) before cutoff at 10 years; (f) after cutoff at 10 years; (g) before cutoff at 20 years; and (h) after cutoff at 20 years.

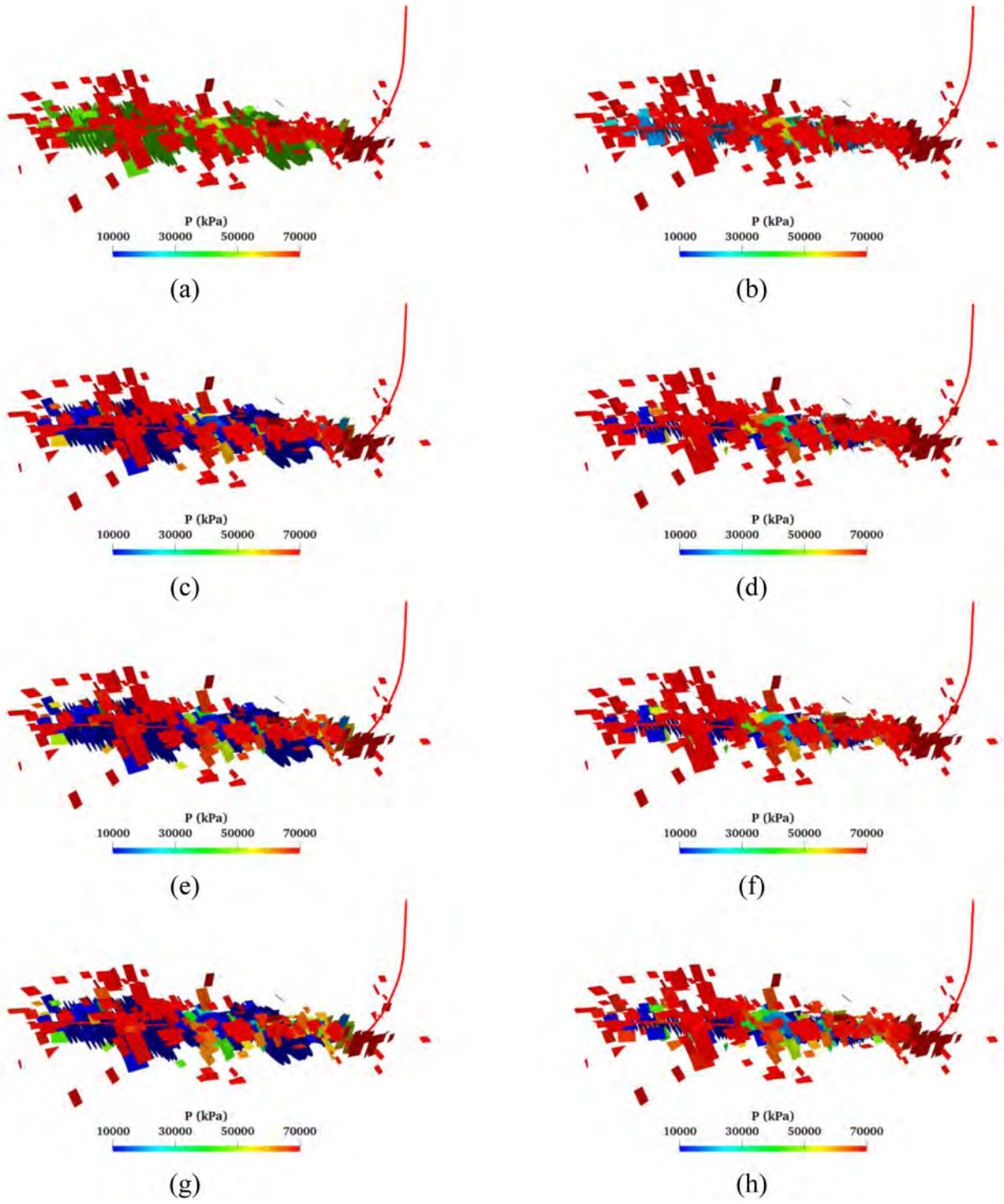

Figure 12—Comparison of fracture pressure drawdown visualizations at different time before and after cutoff calibration: (a) before cutoff at end of history (334 days); (b) after cutoff at end of history (334 days); (c) before cutoff at 5 years; (d) after cutoff at 5 years; (e) before cutoff at 10 years; (f) after cutoff at 10 years; (g) before cutoff at 20 years; and (h) after cutoff at 20 years.

Conclusions

Based on the results of this field case study, we conclude that the proposed microseismic-geomechanics-simulation workflow is robust and flexible to efficiently characterize complex hydraulic fracture properties in a shale gas reservoir with natural fractures. We contrasted the EUR forecasts obtained from the geomechanics simulator and the one obtained using cutoff coefficients and observed a marked difference in

effective fracture geometry. The whole process allows engineers to make informed decisions about future stimulation plans. A summary of key conclusions is discussed below:

1. Using direct estimates of fracture geometry from microseismic data can overestimate fracture geometry because it may contain information of shear failure planes that are distant to the actual hydraulic fracture process.
2. Fracture geometry from hydraulic fracture propagation models can overestimate the effective contribution of hydraulic fractures because values of key geomechanical parameters are uncertain. Additionally, fracture closure could be a factor that reduces fracture half-lengths at the fracture tips, reducing the fracture geometry. Fracture height reduction may respond to the effect of proppant settlement at the fracture, due to gravity, which may leave unpropped regions in the upper parts of the hydraulic fractures.
3. The application of cutoff coefficients is shown to provide reliable and efficient mechanisms to calibrate effective fracture geometry that actually influences production behavior. Moreover, traditional history matching models fail to assess the influence of natural fractures due to incapacities to model them explicitly at the reservoir scale.
4. Satisfactory results attained in this case study motivate the integration of microseismic data with DTS, DAS, and DSS data in order to accurately produce high-fidelity estimates of fracture geometry that could be readily applied for completion optimization.

Nomenclature

SI Metric Conversion Factors

ft	×	3.048	e−01	=	m
ft3	×	2.832	e−02	=	m3
cp	×	1.0	e−03	=	Pa·s
psi	×	6.895	e+00	=	kPa
md	×	1e−15	e+00	=	m2

References

Cipolla, C., L., Lolon, E. P., Erdle, J. C., & Rubin, B. (2010). Reservoir Modeling in Shale-Gas Reservoirs. *SPE Res Eval & Eng* **13** (2010): 638–653. doi: https://doi.org/10.2118/125530-PA.

Ghaderi, A., Taheri-Shakib, J., & Sharifnik, M. A. (2019). The effect of natural fracture on the fluid leak-off in hydraulic fracturing treatment. *Petroleum*, Volume **5**, Issue 1, 85–89.

Hakso, A., & Zoback, M. (2019). The relation between stimulated shear fractures and production in the Barnett Shale: Implications for unconventional oil and gas reservoirs. *GEOPHYSICS* **84**: B461–B469.

Hull, R., Woerpel, C., Trujillo, K., Bohn, R., Wygal, B., Carney, B., & Carr, T. (2020). Hydraulic fracture characterization using fiber optic DAS and DTS data. Paper presented at the SEG International Exposition and Annual Meeting, Virtual, October 2020. doi: https://doi.org/10.1190/segam2020-3425789.1.

Jin, G., Ugueto, G., Wojtaszek, M., Guzik, A., Jurick, D., & Kishida., K. (2021). Novel Near-Wellbore Fracture Diagnosis for Unconventional Wells Using High-Resolution Distributed Strain Sensing during Production. *SPE J.* (2021). doi: https://doi.org/10.2118/205394-PA.

Kumar, S., Rey, A., Dufour, G., & Ogunyomi, B. (2019). Understanding Fluid Flow Behavior in Fractured Reservoir using Dual Porosity Dual Permeability and Discretized Fracture Model. Paper presented at the SPE Annual Technical Conference and Exhibition, Calgary, Alberta, Canada, September 2019. doi: https://doi.org/10.2118/196038-MS.

Rutledge, J., Weng, X., Yu, X., Chapman, C., & Leaney, S. (2016). Bedding-plane slip as a microseismic source during hydraulic fracturing. *SEG Technical Program Expanded Abstracts* : 2555–2559.

Sun, H., Yu, W., & Sepehrnoori., K. (2020). Integrated Fracture Characterization and Flow Profiling with Distributed Temperature Sensing. Paper presented at the SPE Annual Technical Conference and Exhibition, Virtual, October 2020. doi: https://doi.org/10.2118/201619-MS.

Suo, Y., Chen, Z., Rahman, S., & Song, H. (2020). Experimental and Numerical Investigation of the Effect of Bedding Layer Orientation on Fracture Toughness of Shale Rocks. *Rock Mech Rock Eng* **53**, 3625–3635 (2020). https://doi.org/10.1007/s00603-020-02131-1.

Virues, C., & Iheanyichukwu, E. (2016). Improving Understanding of Complex Fracture Geometry of the Canadian Horn River Shale Gas Using Unconventional Fracture Propagation Model in Multi-Staged Horizontal Wells. Paper presented at the SPE Hydraulic Fracturing Technology Conference, The Woodlands, Texas, USA, February 2016. doi: https://doi.org/10.2118/179133-MS.

Wu, K., & Olson, J. (2015). A simplified three-dimensional displacement discontinuity method for multiple fracture simulations. *International Journal of Fracture*. Vol.**193** (02): 191–204.

Xie, J., Tang, J., Yong, R., Fan, Y., Zuo, L., Chen, X., & Li, Y. (2020). A 3-D hydraulic fracture propagation model applied for shale gas reservoirs with multiple bedding planes. *Engineering Fracture Mechanics*. Volume **228**.

Xu, Y., Cavalcante Filho, J. S., Yu, W., & Sepehrnoori, K. (2017). Discrete-Fracture Modeling of Complex Hydraulic-Fracture Geometries in Reservoir Simulators. *SPE Res Eval & Eng* **20** (2017): 403–422. doi: https://doi.org/10.2118/183647-PA.

Yuan, J., Zhou, J., Liu, S., Feng, Y., Deng, J., Xie, Q., & Zhaohui, L. (2017). An Improved Fracability-Evaluation Method for Shale Reservoirs Based on New Fracture Toughness-Prediction Models. *SPE J*. **22** (2017): 1704–1713. doi: https://doi.org/10.2118/185963-PA.